β decay of ^{97}Ag: Evidence for the Gamow-Teller resonance near ^{100}Sn

Z. Hu,[1] L. Batist,[2] J. Agramunt,[3] A. Algora,[3] B. A. Brown,[4] D. Cano-Ott,[3] R. Collatz,[1] A. Gadea,[3] M. Gierlik,[5] M. Górska,[1] H. Grawe,[1] M. Hellström,[1] Z. Janas,[5] M. Karny,[5] R. Kirchner,[1] F. Moroz,[2] A. Płochocki,[5] M. Rejmund,[1] E. Roeckl,[1] B. Rubio,[3] M. Shibata,[1] J. Szerypo,[5] J. L. Tain,[3] and V. Wittmann[2]

[1]*Gesellschaft für Schwerionenforschung, D-64291 Darmstadt, Germany*

[2]*St. Petersburg Nuclear Physics Institute, RU-188-350 Gatchina, Russia*

[3]*Instituto de Física Corpuscular, Dr. Moliner 50, E-46100 Burjassot-Valencia, Spain*

[4]*Michigan State University, East Lansing, Michigan 48824*

[5]*Institute of Experimental Physics, University of Warsaw, PL-00681 Warsaw, Poland*

(Received 11 February 1999; published 23 July 1999)

In two complementary measurements, a cubelike array of 6 Euroball-Cluster germanium detectors and a total-absorption γ-spectrometer were used to investigate the β decay of ^{97}Ag, a three proton-hole nucleus with respect to the ^{100}Sn core. The half-life and Q_{EC} value of the decay of the $9/2^+$ ground state of ^{97}Ag were determined to be 25.9(4) s and 6.98(11) MeV, respectively. A total of 603 γ rays (578 new) was observed, and 151 levels (132 new) in ^{97}Pd have been identified. An interesting β-delayed γ cascade was observed, which comprises 6 γ-transitions with a deexcitation pattern involving an initial increase of the level spin. The Gamow-Teller (GT) β-decay strength distributions from the two measurements reveal a large GT resonance around 4 MeV with a width of about 1.8 MeV. The hindrance factor for the total GT strength, summed from the ground state up to 6 MeV excitation energy in ^{97}Pd, amounts to 4.3(6) with reference to a shell-model prediction. This factor is discussed in comparison with a core polarization and a Monte Carlo shell-model calculation. [S0556-2813(99)05208-5]

PACS number(s): 23.40.−s, 27.60.+j

I. INTRODUCTION

Since the the identification of the doubly closed-shell nucleus ^{100}Sn and some of its neighboring isotopes [1,2], the study of these very neutron-deficient isotopes has attracted considerable interest. The experimental progress in this field includes, e.g., the measurement of the mass of ^{100}Sn and ^{100}In [3], the in-beam spectroscopy of ^{99}Cd [4] and ^{98}Cd [5], the observation of proton radioactivity for ^{105}Sb [6] and ^{112}Cs [7], and the β-decay studies of ^{94}Ag [8], $^{100-104}$In [9–11], and ^{101}Sn [12].

In particular, the unique nuclear structure features of nuclei in the region below ^{100}Sn make β decay interesting, as it is characterized by a fast $\pi g_{9/2} \rightarrow \nu g_{7/2}$ Gamow-Teller (GT) transition (here only the nuclei situated in the ''south-east'' of ^{100}Sn are considered). Within the extreme single-particle shell model, such transitions involve protons in the mostly filled $g_{9/2}$ orbit, with the corresponding GT partner shell $\nu g_{7/2}$ being mostly empty. This model predicts the total GT strength, summed over all the final states, to be

$$\Sigma B(\mathrm{GT}) = \frac{N_{9/2}}{10}\left(1 - \frac{N_{7/2}}{8}\right) B_0(\mathrm{GT}), \qquad (1)$$

where $N_{9/2}$ denotes the number of protons filling the $g_{9/2}$ orbit, $N_{7/2}$ the corresponding value for the $g_{7/2}$ orbit, and $B_0(\mathrm{GT}) = 17.78$ the $\Sigma B(\mathrm{GT})$ value of ^{100}Sn. However, the $\Sigma B(\mathrm{GT})$ values obtained from experiments are significantly smaller than those from theoretical predictions. This ''hindrance'' or ''quenching'' of GT transitions can be expressed as the ratio between the theoretically and experimentally determined GT strengths. For example, a GT hindrance factor of the order of 4 has been found [13] for the $N = 50$ even-even nuclei ^{96}Pd and ^{98}Cd by comparing shell-model predictions with the experimental $B(\mathrm{GT})$ values for β-decay.

In an attempt to explain the observed GT hindrance, Towner [14] has considered the effects of pairing correlations, core polarization and higher-order configuration mixing. As we will discuss below, the core-polarization and higher-order effects are both large and together can account for most of the observed hindrance. However, one probably needs correlations between the $0g_{9/2}$ and $0g_{7/2}$ orbitals which go beyond the core-polarization model, such as those incorporated in the recent Monte Carlo shell-model calculations [15], in order to fully account for the observed hindrance.

The GT strength can be experimentally determined by measuring β-delayed particles and γ rays. The electromagnetic radiation is normally measured with high-resolution germanium detectors. However, in the cases of odd-even and odd-odd nuclei with high Q_{EC} values, it is expected that a significant part of the total β-decay strength is distributed over many daughter states at large excitation energy, where the level density is very high. Since the β feeding to individual levels is often very weak, and moreover the γ deexcitation might proceed through several partly parallel cascades, standard high resolution γ-γ spectroscopy is generally insufficient to determine the complete GT-strength distribution due to its limited detection sensitivity.

Alternatively, the β strength can be obtained from total-absorption spectrometry by using 4π detectors. A highly advanced version of a total-absorption spectrometer (TAS) has been installed at the mass separator on-line to the heavy-ion accelerator UNILAC of GSI [16] for studying the β decay of nuclei around the doubly magic nucleus ^{100}Sn and around the semimagic nucleus ^{146}Gd. This instrument consists of a

large NaI (γ ray) detector, and includes a germanium (x ray) detector as well as silicon (β^+) detectors. First TAS studies of the β decay of ^{103}In [11] and ^{150}Ho [17] have recently been completed.

Since the TAS technique is based on recording cascades of β-delayed γ rays, and the energy resolution of NaI detectors is poor compared with germanium detectors, the evaluation of TAS data depends strongly on the knowledge of the response function of the TAS spectrometer for each particular cascade. The information required to obtain the response function concerns excited levels and their deexcitation pattern, which can be determined from high-resolution experiments. Thus, the ''double strategy'' of combining high- and low-resolution studies provides a tool to map the GT-strength distribution to high excitation energies in the daughter nucleus (see Ref. [17] for more details).

As part of an ongoing research program on β decays near ^{100}Sn, we investigated ^{97}Ag. This nucleus is characterized by a predominant configuration of three proton holes in the $g_{9/2}$ orbit and a full $g_{9/2}$ neutron shell. On the basis of the extreme single-particle model, one expects the decay of ^{97}Ag to be dominated by a decay which mainly populates, after breaking a $\pi g_{9/2}^2$ pair, the three-quasiparticle states $(\pi g_{9/2}^{-2} \nu g_{7/2})$ in ^{97}Pd at excitation energies around 4 MeV [13].

We studied the decay of ^{97}Ag by using both complementary spectroscopic tools mentioned above, i.e., TAS as a low-resolution high-efficiency device and a cube-like array of six Euroball Cluster germanium detectors (Cluster Cube) [18]. The unique features of the latter array, including a very high photopeak efficiency even at relatively high γ-ray energies, high resolution and high granularity, offered an unprecedented opportunity to obtain high-quality β-decay data.

In this paper, we introduce the experimental techniques in Sec. II and then report on the experimental data obtained from the Cluster Cube and TAS measurements in Sec. III and Sec. IV, respectively. In Sec. V, we compare the results obtained from both techniques. A shell-model calculation is discussed in Sec. VI, in comparison with experimental results. Finally, a summary is given in Sec. VII.

II. EXPERIMENTAL TECHNIQUES

The experiment was performed at the GSI on-line mass separator. ^{97}Ag was produced in fusion-evaporation reactions using 4.0 and 4.3 MeV/nucleon beams of ^{40}Ca of 50–80 particle$\times$nA intensity from the UNILAC on a 3 mg/cm^2 ^{60}Ni target, enriched to 99.08%. The reaction products were stopped in a graphite catcher inside a FEBIAD-B2C [19] ion source which, due to its moderate operation temperature of 1800 K, perfectly handles the volatile element silver, but considerably suppresses the refractory contaminants palladium and rhodium. After ionization, acceleration to 55 keV, and mass separation in a magnetic sector field, the $A=97$ ions were implanted into a moving tape collector. After a pre-selected collection time, the tape moved the implanted activity through a differentially-pumped slit system out of vacuum into the center of the detector systems, where it was measured while in vacuum the next source was collected.

For the experiment with the Cluster Cube a collection/measurement cycle of 40 s was applied to optimize the ^{97}Ag decay rate and to suppress the longer-lived contaminants ^{97}Pd and ^{97}Rh even further. In this experiment, for a period of about 54 hours, the ^{97}Ag beam intensity was about 400 atoms/s at a ^{40}Ca beam intensity of 65 particle$\times$nA. The accumulation of γ-singles and γ-γ coincidence data in the Cluster Cube measurements was triggered by a logic *or* condition of all timing signals of all capsules. The other three kinds of triggers described in Ref. [18] were not used in this work. Another type of singles γ spectra were recorded by selecting individual germanium detectors from the Cluster Cube and accumulating the so-called MR2000 spectra (see Ref. [18] for the definition). The corresponding dead-time correction was negligible since the dead-time involved in the MR2000 data acquisition system amounted to only a few microseconds per event in comparison to a few hundred microseconds in case of the list-mode data.

For the TAS experiment, due to its low resolution and total-absorption feature, the suppression of the isobaric contamination is more important than for the Cluster Cube. Therefore, the ion source was operated in the so-called ''bunch'' mode [20] by accumulating the silver activity for 54 s in a cooled pocket inside the ion source and releasing it as a bunch of 1.6 s FWHM by shortly heating the pocket. This ''chemical separation'' mode reduces the ^{97}Ag rate, but only by a factor of 2, whilst the contaminants are attenuated by a factor of at least 34. A collection/measurement cycle of 56 s was chosen. After three consecutive collection periods in TAS, the $A=97$ beam was directed for a 56 s interval to a separate tape collector which was used for monitoring intensity and purity of the source by γ-spectroscopy with a standard-size germanium detector, while simultaneously a background measurement was performed at TAS. This mode of beam sharing between TAS and the monitoring station was continued for a total counting time of about 32 hours.

III. RESULTS FROM THE CLUSTER CUBE MEASUREMENT

A. γ-ray singles spectrum

Figure 1 shows the γ-singles spectrum retrieved from the list-mode data, which contains 2.7×10^8 events. This spectrum is rather complex for several reasons. First, there are sizable contributions from isobaric contaminants and room background. Secondly, as can be seen from the γ-coincidence analysis described in Sec. III B, the occurrence of multiply-placed γ rays is common over the whole energy range of interest. Finally, the summing effect of strong γ rays and the escape effect of high-energy γ rays add to the complexity of the spectrum. Because of the complexity of the spectrum, only a few representative γ-rays from the ^{97}Ag decay are labeled by their energies in keV. In addition, contributions from isobaric contaminants (^{97}Pd, ^{97}Ag), from room background (BKG) or from escape effects (ESC) are marked.

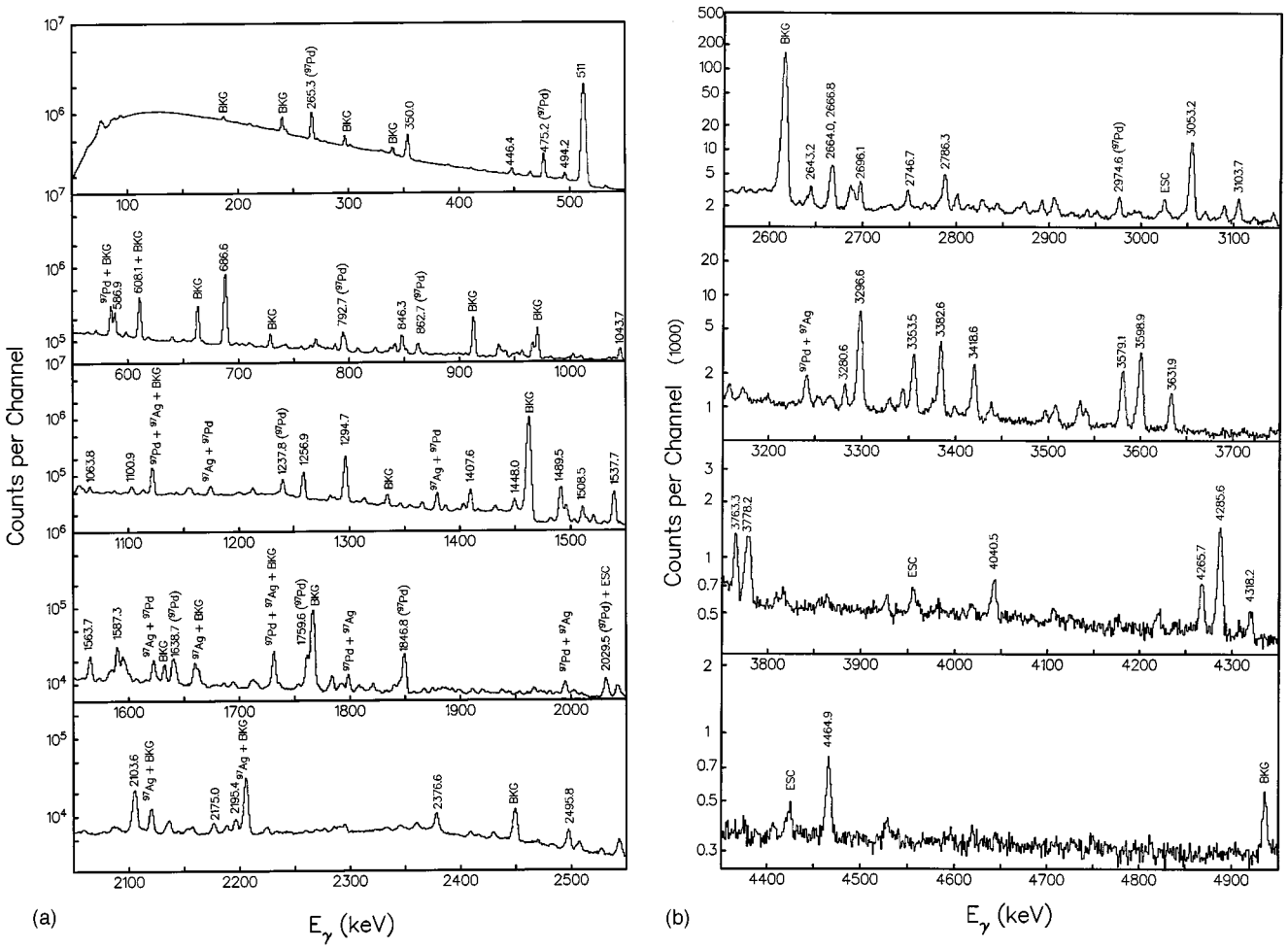

FIG. 1. γ-ray singles spectrum obtained by using the 42 capsules of the Cluster Cube for the measurement of mass-97 samples. See text for details.

B. Coincidence spectra

We obtained 1.1×10^8 γ-γ coincidences from the Cluster Cube measurement by using the trigger mentioned above. In Fig. 2, a representative coincidence spectrum gated on the 686.6 keV γ-ray transition is shown. Because of the complexity of the spectrum, only a few representative γ-rays from the ^{97}Ag decay are labeled by their energies in keV. In addition, contributions from escape effects (ESC) and an artificial peak ($\times$) are marked. The latter is related to a 1461 keV background γ-ray (^{40}K), and occurs when the gate comprises energy depositions: (i) either from the primary Compton scattering of this γ-ray in one of the Cluster Cube capsules, or (ii) from full absorption of this Compton radiation in another capsule. The cusp-like structures appearing in the spectrum originate from setting the background gates in regions where coincidences with the 686.6 keV γ-ray transition occur. Figure 3 shows the weakest γ ray identified in this work, which was determined to have an intensity value of 0.008% per β decay of ^{97}Ag. In the previous work using standard germanium detectors [21], the weakest γ ray placed in the decay scheme was the 637.7 keV γ-line with an intensity value of 1.3%. This factor of 160 indicates the considerable improvement of the detection sensitivity obtained in this work.

C. Half-life determination

As can be seen from Table I, 16 γ-lines were chosen for the analysis, which leads to the weighted average of 25.9(4) s. This result is in good agreement with the value of 25.3(3) s determined previously [21], except for the 1044 keV γ-line. This γ line was previously assigned [21] to the β decay of the ^{97}Ag isomeric state because of its shorter half-life [17.4(21) s]. However, the present work yields a half-life value of 22(4) s for this γ-line, which agrees with the values obtained for the other γ-lines, indicating that it originates from the ^{97}Ag ground-state decay. This observation is consistent with the placement of this γ-transition in the decay scheme (see Sec. III D).

D. Proposed decay scheme

1. γ transitions

The decay scheme for ^{97}Ag [22] as obtained from this work includes 603 γ-lines in total (578 new) and 151 excited states of ^{97}Pd (132 new). The intensities of the γ lines in units of ''% per β decay of ^{97}Ag'' were determined by assuming the summed intensities of all observed γ transitions to the ^{97}Pd ground state to represent 100%. The uncertainty

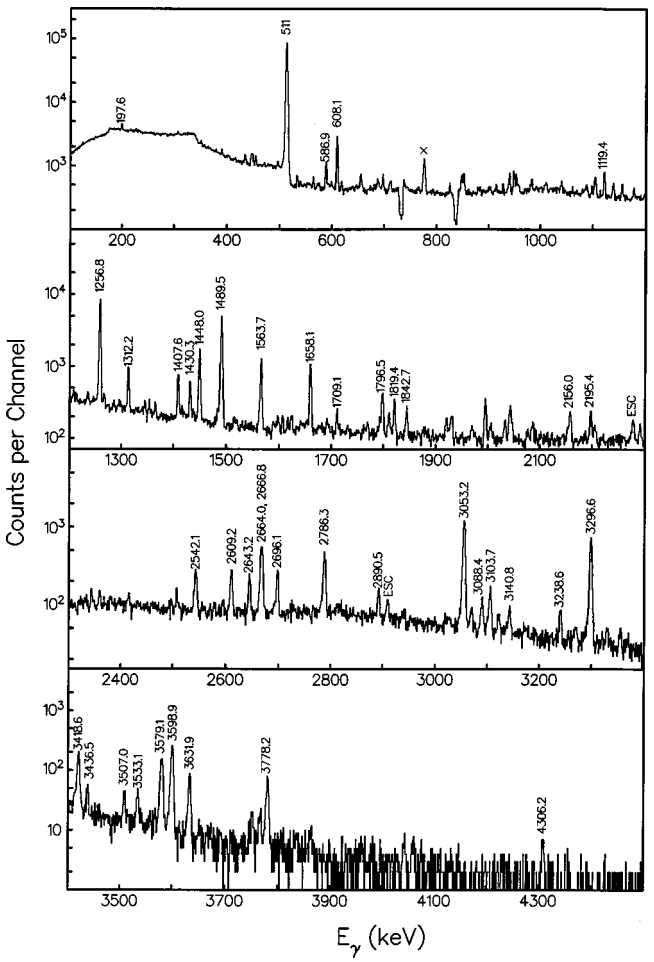

FIG. 2. Background-subtracted coincidence spectrum from the Cluster Cube data, gated on the 686.6 keV γ-ray transition. See text for details.

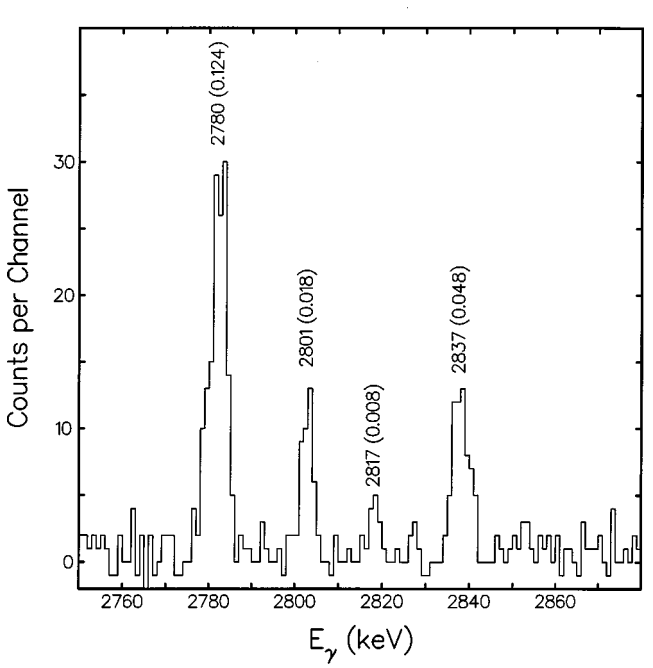

FIG. 3. Part of the background-subtracted coincidence spectrum from the Cluster Cube data, gated on the 1537.7 keV γ-ray transition, showing the 2817.1 keV γ-ray transition which is the weakest γ-line from the ^{97}Ag decay identified in this work. The γ-ray intensity values in % per β decay of ^{97}Ag are given within brackets following the transition energies in keV.

of this normalization was considered negligible due to the fact that the intensities of such ground-state transitions were measured with an efficiency-related uncertainty of only 5% [18], and that even very weak lines were detected [e.g., 0.025(8)% for the 4618.2 keV line] [22]. The decay scheme of ^{97}Ag [22] contains only those γ transitions that were found to be in coincidence with 511 keV γ-quanta and for which the respective initial and final levels were confirmed by other γ-transitions. Whenever possible, the coincidence assignments were checked for intensity by comparison with the singles intensities; however, many γ rays were observed unambiguously only in the coincidence spectra. Due to the contamination from room background and isobars, the assignment of some γ rays was additionally based on the half-life information. This procedure was implemented by sorting the events (singles or matrices) into four subsequent time subgroups within the 40 s counting interval (see Sec. II) and then comparing the γ intensities accumulated in the subgroups. If a given γ-intensity value showed a decreasing time-function, the corresponding γ ray was assigned to the ^{97}Ag decay, otherwise to the contaminants. For weak γ lines, the placements were also checked by using the matrix which was obtained. In this mode, the pulse heights of directly neighboring capsules within each Cluster Cube detector are summed (see Ref. [18] for more details).

The γ-γ coincidence matrix sorted in the add-back mode was not used for determining the γ-ray intensities, due to the

TABLE I. γ-ray transitions used for the determination of the half-life of ^{97}Ag.

E_γ (MeV)	$T_{1/2}$ (s)
446.4	24(5)
586.9	29.4(13)
686.6	25.9(45)
846.3	34(6)
1043.7	22(4)
1211.0	22(4)
1256.8	22.6(21)
1294.7	27.3(12)
1448.0	36(11)
1489.5	25.3(10)
1537.7	25.5(18)
1563.7	27(6)
1658.1	21.0(27)
2666.8	22(3)
3053.2	25(5)
3296.6	26(5)
Average	25.9(4)

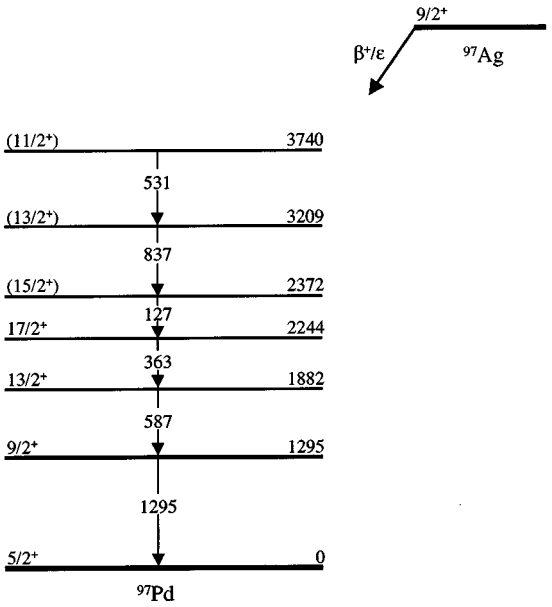

FIG. 4. High-multiplicity γ-ray cascade observed from the Cluster Cube data, with a high-spin state ($17/2^+$) in ^{97}Pd being populated. For the deexcitation of the 3740 keV state in ^{97}Pd, only the cascade involving the high-spin state ($17/2^+$) is shown, other deexcitation cascades are omitted.

complexity introduced by the summing effect. The intensities were determined by using either the γ-singles spectrum or γ-γ coincidence data [18]. The summing peaks and single- and double-escape peaks were excluded, but the summing correction for γ-ray intensities was not applied since the total γ-detection efficiency of an individual capsule is so small that the summing effect can be safely neglected [18].

The intensities for γ rays with energies below 350 keV were corrected for internal conversion, while for those with higher energies these corrections become small ($<1.5\%$) and were thus neglected. For these corrections, the transitions were assumed to be of type $M1$, except for the 305.5 keV transition (from $13/2^+$ to $9/2^+$) which was assigned to be of pure $E2$ type [23].

An average γ-cascade multiplicity of 2.43(3) was obtained by summing all γ-ray intensities and then dividing by the total intensity of γ transitions to the ground state of ^{97}Pd. It is worth noting that, as shown in Fig. 4, the highest γ-cascade multiplicity observed in the β decay of ^{97}Ag amounts to 6. This cascade is further discussed in Sec. III D 2.

2. Levels in ^{97}Pd

The ^{97}Pd level energies were determined from the energies of the depopulating γ rays and the energies of the corresponding lower levels. This procedure relied heavily on the accurate energy calibration [18] and on the high quality of the coincidence data. Consequently, not only the intensities of many multiply-placed γ-transitions were suitably distributed, but also a few groups of states in ^{97}Pd have been identified that each exhibit small level-to-level distances. The closest-lying levels identified in this work have an energy separation of only 0.8 keV, the corresponding level energies being 2375.8 keV and 2376.6 keV. While the 2375.8 keV state is populated mostly from the 3740.0 keV level through the 1364.1 γ-transition and decays mainly to the 1881.6 keV level through the 494.2 keV γ-transition, the 2376.6 keV level decays dominantly to the ground-state directly by a γ-transition that is not observed in coincidence with the 1364.1 keV γ-ray transition.

We were able to assign spins and parities to states in ^{97}Pd [22] from a combination of arguments. The spins and parities of the ground-state of ^{97}Pd and of excited ^{97}Pd levels at 686.6, 1294.7, 1881.6 and 2244.3 keV have been previously assigned [24] to be $5/2^+$, $7/2^+$, $9/2^+$, $13/2^+$ and $17/2^+$, respectively. Based on these results, the proposed values of $9/2^+$ for the ^{97}Ag ground-state [25] and of $11/2^+$ ($13/2^+$ or $11/2^+$), $9/2^+$, and $13/2^+$ for the excited ^{97}Pd levels at 1943.4, 2141.1, 2176.1, and 2481.9 keV [23], respectively, were confirmed. In addition, we assigned spins and parities to ^{97}Pd levels according to the β intensities from the ^{97}Ag decay and the relative γ intensities. The case of the $1/2^+$ state at 775.0 keV is discussed in Sec. VI C. This procedure was based on the following three assumptions

(1) A β decay with a log ft value smaller than 6.0 represents an allowed GT transition, which confines the spin and parity of the populated daughter level to be $7/2^+$, $9/2^+$, or $11/2^+$.

(2) The γ-transition does not change the parity of the connected levels.

(3) Competition of $E2$ and $M1$ deexcitation of a given level occurs only if the ratio of the reduced $E2$ and $M1$ transition strengths, as deduced from the respective Weisskopf estimates, fulfills the condition $B(E2)/B(M1) \geqslant 10^{-2}$.

We observed a few high-spin states in ^{97}Pd, namely a $17/2^+$ state at 2244.3 keV, confirming the data given in [24], and two $15/2^+$ states at 2371.6 keV and 2500.5 keV, respectively. This indicates an interesting γ-cascade decay pattern shown in Fig. 4. The $11/2^+$ state, which is strongly populated by β decay, deexcites through states with higher spins, and then after several steps ends up with states with lower spins. The observation of a high-spin ($17/2^+$) state in β decay of a low-spin ($9/2^+$) nucleus shows again the excellent detection sensitivity of the Cluster Cube. The cascade represents only 0.033% out of the total 14.9% β-feeding of the 3740 keV state, which is far below the detection limit for $\gamma\gamma$ coincidences in a standard two-germanium detector setup [21]. From a singles spectrum in such a setup one could at best place, in addition to the intense 587 and 1295 keV transitions, the well known [24] 363 keV transition. This would imply an apparent direct β branch to the $17/2^+$ state and hence lead to erroneous conclusions for the spin assignment to the parent state.

3. Comparison with previous work

The following major differences occur between the ^{97}Ag decay-scheme obtained in this work and that proposed previously [21].

(1) The γ-ray energies determined from both works differ in some cases, the discrepancies reaching even values beyond 2 keV and thus resulting in sizably different level energies. On the one hand, this difference can be related to the insufficient sensitivity of the detection setup applied in the previous work and to the corresponding restriction in disentangling multiply-placed γ-transitions. On the other hand, the energy calibration in the previous work for the intermediate to high-energy region is less accurate in comparison with this work in which we performed the energy calibration by using various γ-sources with energies from tens of keV up to 6 MeV [18].

(2) In the previous work, two γ-lines were not correctly placed in the decay scheme. The 1880.7 keV γ-line cannot be assigned to a transition between the 1880.7 keV state and the ground state of ^{97}Pd, because a previous in-beam work [24] has determined the spins for these two states to be $13/2^+$ and $5/2^+$, respectively. Furthermore, the observation of an $M3$ transition, in competition to an allowed $E2$ branch, is ruled out. The other γ-line interpreted incorrectly has an energy of 1151.3 keV and was misassigned to connect the 3291.3 keV level (such a level was found in our work) and the 2140.0 keV level (the energy of this level was determined to be 2141.1 keV in our work). Our results based on considerably improved coincidence data show that these two γ-lines actually belong to two groups of multiply-placed transitions (see Ref. [22] for details).

(3) We have found that most of the γ-lines are multiply-placed in the decay scheme (see Ref. [22] for details), whereas the previous work was unable to identify any doublets.

(4) There is a misprint in the level energy of 3323.4 keV given in [21] which corresponds to a value of 3353.7 keV in our work.

(5) Most importantly, we have identified numerous new γ rays from the ^{97}Ag decay and numerous new ^{97}Pd levels. This is about an order of magnitude more levels and γ rays than were formerly observed, commensurating with the improvement of observation sensitivity. In particular, as already mentioned in Sec. III C, the 1043.7 keV γ-transition, which was tentatively assigned to the decay of the ^{97}Ag isomeric state in the previous work [21], has been placed unambiguously in the decay scheme of the ^{97}Ag ground state, this assignment being confirmed by rich coincidence information.

E. β-intensity distribution

The β intensities I_β, which are given in units of ''% per β decay of ^{97}Ag'' [22], were obtained by using the γ-intensity balances. Some very small I_β values, which have very large uncertainties, indicate the absence of a GT transition for the corresponding ^{97}Pd level and are thus not included in [22]. For example, the 1881.6 keV ($13/2^+$) and 2244.3 keV ($17/2^+$) levels were determined to have I_β values of 0.098(0.809)% and $-0.093(0.036)$%, respectively. As the corresponding β-transitions are not of allowed character, this observation confirms the correctness of the intensity balances.

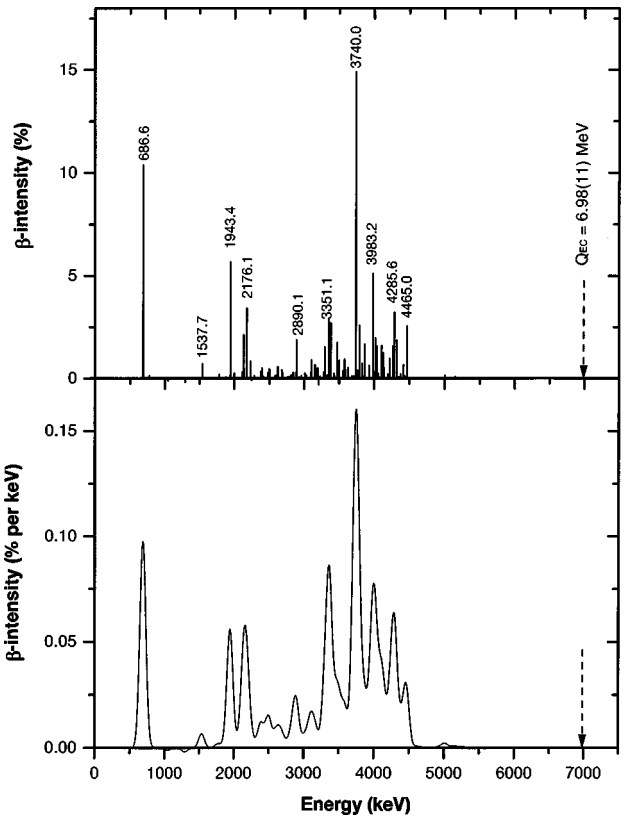

FIG. 5. β-intensity distribution for the ^{97}Ag decay obtained from the Cluster Cube measurement. The upper panel shows the result level by level in histogram form, where some representative levels are labeled with energies in keV. The lower panel presents the result smoothed by using a Gaussian function with a FWHM of 100 keV. The experimental Q_{EC} value is indicated by arrows.

The I_β distribution obtained from the Cluster Cube data is shown in Fig. 5. The lowest excited state in ^{97}Pd (686.6 keV) receives 10.4(9)% of the β feeding with a log ft value of 5.85(6). Up to 1943.4 keV, only very weak β feeding was observed. The 1943.4 keV level ($11/2^+$) is obviously fed by an allowed GT decay, as indicated by the rather large I_β value of 5.7(6)% and by the rather small log ft value of 5.59(7). The next states strongly populated by GT decays lie at 2134.7 keV ($7/2^+$, $9/2^+$) and 2176.1 keV ($9/2^+$), which receive 2.1(3)% and 3.4(8)% of the β feeding with log ft values of 5.92(7) and 5.69(8), respectively. Between 2176.1 keV and 2890.1 keV, no sizable β feeding was observed. The 2890.1 keV state ($11/2^+$) is again fed by an allowed GT decay with an I_β value and a log ft value of 1.9(2)% and 5.57(7), respectively.

One of the most remarkable results of this work is the observation of a resonance-like β feeding at ^{97}Pd excitation energies between 3 and 4.8 MeV. This represents a major progress over the previous work [21] which only reached the tail of this resonance. Receiving about 67% of the β feeding, this resonance is characterized by five groups centering at 3351, 3740, 3983, 4286, and 4465 keV, respectively. The ^{97}Pd state that is most strongly populated by the β decay of ^{97}Ag is situated in the middle of the resonance: It is the

3740.0 keV state ($11/2^+$) with an I_β value of 14.9(8)%, corresponding to the smallest log *ft* value of 4.12(8) found in this work. Above 5 MeV, several states were observed with a total I_β value of about 0.4%. The highest-lying state identified in this work has an excitation energy of 5326.2 keV. This state has an I_β value as low as 0.015(5)%, but has nevertheless a log *ft* value of 5.98(16), which represents weak evidence for allowed GT decay.

IV. RESULTS FROM THE TAS MEASUREMENTS

A. Experimental TAS spectra

By demanding coincidences between the NaI signals and palladium x rays recorded by the TAS germanium detector [16], about 2.2×10^4 events corresponding to the electron-capture (EC) mode of the ^{97}Ag decay were selected. The coincidence of the TAS signals with those from one of the two silicon detectors, situated in the center of TAS [16], was used to select the β^+ component of the ^{97}Ag decay. The total of 1.5×10^6 events were accumulated for this decay mode. The spectrum accumulated in coincidence with the upper silicon detectors included about 7×10^5 events.

^{97}Pd decay events were not harmful to the EC-component spectrum of the ^{97}Ag decay, but contributed considerably to that corresponding to the β^+ component. In order to obtain a TAS spectrum containing pure ^{97}Ag β-activity, we additionally measured the decay of ^{97}Pd in a separate experiment and then subtracted it from the total TAS spectrum for β^+ decay. The normalization factor for this procedure was calculated by using the intensity of rhodium x rays recorded by the germanium detector of TAS. The TAS spectra were corrected for the pile-up effect caused by random summation [26]. Due to the registration of γ quanta in the silicon counters, the initial silicon-gated spectrum contained a contribution from the EC decay. In order to remove this contribution, we simulated such events by using results from the Cluster Cube data analysis, and corrected the β^+-decay TAS spectrum correspondingly. Using the method described in Sec. 3.3.4 of [11], we derived an overall EC/total ratio of 0.276(15) for the β decay of ^{97}Ag.

B. Simulated TAS spectra

As shown in Fig. 6, we have also calculated TAS spectra by using the decay scheme established from the Cluster Cube data and the simulated TAS response to γ rays and positrons. The method for obtaining the simulated TAS spectra is described in detail in [27]. We used the code SIGMA [28] that was originally developed for a simulation of γ-quanta transport, but treated the positron-transport under some simplifying assumptions which limit the accuracy in calculating the contribution of positrons to the total energy deposition. A comparison with a simulation performed by using the code GEANT3 [29] has shown that these approximations lead to differences in peak efficiencies of up to 5%. The simulation was performed by assuming a Q_{EC} of 6.98(11) MeV for the decay of ^{97}Ag (see Sec. IV D) and by using the decay scheme deduced from the Cluster Cube data analysis. Figure 6 shows that a good overall agreement between the results

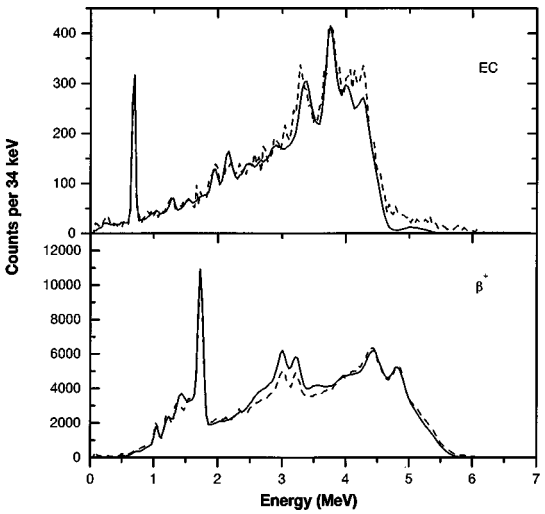

FIG. 6. Experimental TAS spectra related to the EC component (upper panel, dashed line) and the β^+ component (lower panel, dashed line) of the ^{97}Ag decay, in comparison with the spectra simulated by using the decay scheme established from the Cluster Cube data (solid lines). The normalization between experiment and simulation was achieved on the basis of the *total* number of EC and β^+ events, with the experimental efficiency for EC and β^+ detection being taken into account. Note that peaks in the β^+ spectrum occur 1.022 MeV above the positions of the corresponding peaks in the EC spectrum.

from the simulation and the TAS data has been reached. However, it is evident from this figure that the high-resolution experiment missed γ rays emitted from the high-energy region above about 4 MeV. In particular, the difference between the experimental and simulated TAS data becomes relatively large at the high-energy end of the EC spectra, i.e., above 4.7 MeV. Some events appear above 5.5 MeV in the experimental EC-spectrum, where the simulation does not yield any. This inability of the Cluster Cube to detect γ rays emitted from high-energy states results in an incorrect determination of I_β values. This is due to the fact that too small I_β values are deduced for levels deexcited by unobserved γ rays, while excessive population is obtained for those levels which are fed by these γ transitions. Since the EC/total ratio varies strongly with the excitation energy, this excess is more apparent in the β^+-decay spectrum, as can be observed in Fig. 6, in particular for ^{97}Pd excitation energies between 1.7 and 3 MeV (note the energy shift of the β^+ spectrum compared to the EC one).

C. Deconvoluted TAS spectra

We used the decay scheme of ^{97}Ag, established from the Cluster Cube data, as a basis for constructing the response matrix of the TAS and for analyzing the experimental TAS spectra by means of the peel-off method discussed in Ref. [11]. In addition, the response matrix has to assume the γ-deexcitation branching ratios for levels in the energy region where excessive events occurred in the experimental TAS spectra compared to those simulated by using the Cluster Cube data. Because of the poor energy resolution of the

TAS, we were unable to resolve individual levels, and therefore used an averaged response matrix, with each energy bin in the deconvoluted TAS spectra being treated as a level [11]. For the region below 4 MeV, where a relatively good agreement between the simulated and experimental TAS spectra was obtained, we constructed a response matrix by using the γ-deexcitation branching ratios derived from the Cluster Cube data analysis. In the high-energy region, several assumptions concerning the γ-deexcitation branching ratios had to be made, which will be discussed in the following.

We define $I_\gamma(E)$ as the summed intensities of γ rays emitted from a level with an excitation energy E. As dipole γ-transitions are probably dominant in the γ-deexcitation cascades, we assumed that the branching ratio $b_{i,k}$ for a γ transition from energy bin i to k has a cubic energy dependence, $b_{i,k} \propto b_k \cdot (E_i - E_k)^3$. For each energy bin the branching ratios were normalized to unity. In choosing the factors b_k, we assumed that the Cluster Cube data analysis had correctly determined the $I_\gamma(E)$ for the levels observed in the low-energy region, since it involved only summing intensities of individual γ rays but not the γ-intensity balance. However, these values can also be calculated during the procedure of deconvoluting the TAS spectra and calculating the I_β distribution. During this procedure it is required that the $I_\gamma(E)$ distributions obtained from the Cluster Cube data and the TAS data should be in agreement, as the γ intensities that remained unobserved in the Cluster Cube experiment are comparatively small (see Sec. III D 1).

The deconvolution of TAS spectra was achieved by performing a series of iterations. We started with the assumption that the b_k values are the same for all levels except the ground state and the lowest-lying levels of ^{97}Pd. For these states we chose b_k values by assuming that the corresponding γ-branches are close to those observed in the Cluster Cube experiment. With this assumption, we calculated the response matrix and deconvoluted the EC and β^+ spectra by applying the peel-off method [11]. Then we adjusted the coefficients b_k to minimize the difference between the $I_\gamma(E)$ distributions obtained from the Cluster Cube data and the TAS data, respectively, while checking the physical constraints on EC- and β^+-intensity distributions [11]. After the first iteration we found the maximum disagreement to occur in the excitation-energy region $2.0 < E < 2.5$ MeV, where the $I_\gamma(E)$ values calculated during the deconvolution procedure turned out to be much smaller than those from the Cluster Cube data analysis. In the next iterations we adjusted the coefficients b_k in such a manner that this difference disappeared. The distribution for $I_\gamma(E)$ obtained from the deconvolution of the TAS data is shown in Fig. 7 together with that obtained from the Cluster Cube data. It should be noted that the total area under each of the $I_\gamma(E)$ distributions displayed in Fig. 7 is equal to the average number of γ quanta per decay of ^{97}Ag.

The I_β distribution obtained from the deconvolution is shown in Fig. 8 as the sum of EC and β^+ components, normalized by using the EC-branching ratio deduced above. In the same figure the folded distribution obtained from the

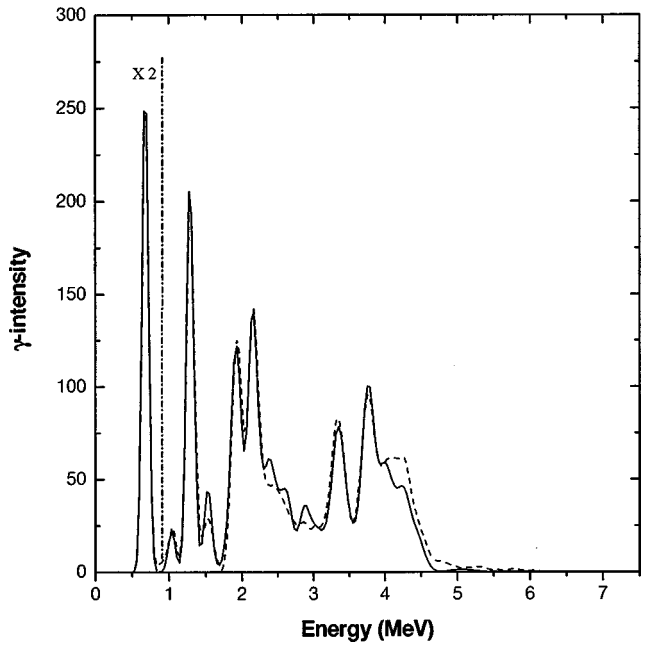

FIG. 7. Intensities of β-delayed γ rays from the ^{97}Ag decay as a function of ^{97}Pd excitation energy. The intensities are given in units of quanta/MeV emitted per 100 ^{97}Ag β-decays. The TAS results (dashed line), deduced by using the peel-off method, are compared to the results from the Cluster Cube measurement (solid line). The latter distribution has been folded with the TAS resolution. Note that the intensity values below 0.86 MeV have been reduced by a factor of 2.

Cluster Cube data analysis is displayed. It is evident that the difference between the $I_\beta(E)$ data obtained from Cluster Cube and TAS measurements, respectively, resembles the features that have already been observed in Fig. 6.

The uncertainties of I_β values from the TAS measurement are dominated by systematic uncertainties [11] over statistical contributions in the region below 4.5 MeV, having a relative value of about 10% in the energy region $1.7 < E < 4.5$ MeV, where the I_β values are high. For lower energies, the uncertainties of the deconvolution procedure accumulate, including also those from the simulation of positron transport [11]. The variation of the coefficients b_k, under the condition that the agreement remains satisfactory, leads to systematic I_β uncertainties below 7%. The width of the bins was chosen to be about 34 keV. The resulting nonphysical small I_β values (about 1% in total) in the region around 1 MeV are due to the uncertainties from both the simulation of TAS response and the peel-off method. Therefore, we assumed additional uncertainties of at least about 2% per MeV for the I_β values in the energy region where the I_β values are large. The statistical uncertainties of the I_β value become important for the region $E > 4.5$ MeV, being about 10% for a 100 keV bin at 5 MeV and about 50% for a 100 keV bin at $E > 6$ MeV.

D. Determination of the Q_{EC} value

In order to deduce the Q_{EC} value of ^{97}Ag we determined the experimental EC/β^+ ratios within the excitation-energy

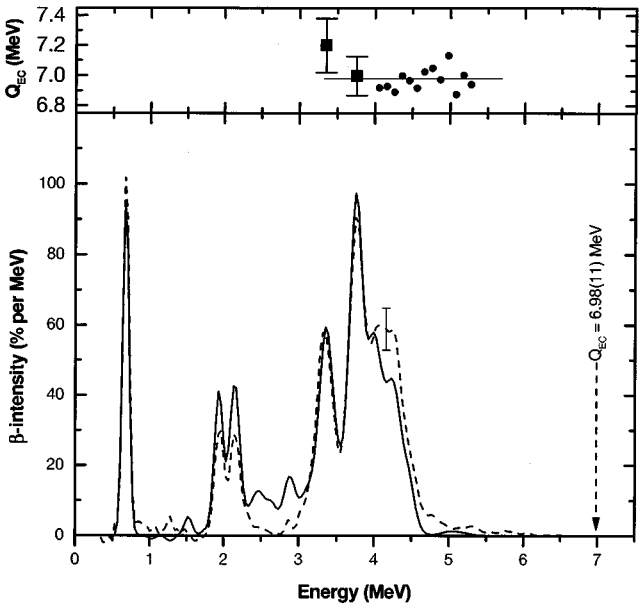

FIG. 8. Lower panel: β-intensity distributions for the ^{97}Ag decay obtained from the TAS data (dashed line) and from the Cluster Cube data (solid line). The latter results were adapted to the TAS resolution by a smoothing procedure. The uncertainty shown for the TAS result at 4.2 MeV represents the uncertainty for a bin size of 100 keV. The experimental Q_{EC} value is indicated by an arrow. Upper panel: Q_{EC} values deduced from the experimental EC/β^+ ratios for selected ^{97}Pd excitation energies. The uncertainties of the Q_{EC} determination are exemplified for the 3.3 and 3.8 MeV data. The weighted average of 6.98(11) MeV obtained for the Q_{EC} value is indicated by a horizontal line (see text).

interval $3.0 < E < 5.3$ MeV, where both EC and β^+ intensities are sufficiently strong. The theoretical relation between the EC/β^+ ratio and the decay energy for allowed β decay was taken from [30]. For this procedure we selected two strong peaks of the I_β distribution at 3.3 MeV and 3.8 MeV as well as 34 keV bins within the tail of this distribution above 4.0 MeV (see Fig. 8). The low-energy range was *not* considered as it is characterized by small EC contributions. The individual Q_{EC} values as well as the weighted average of 6.98(11) MeV are given in Fig. 8. The uncertainties involved in this procedure take into account contributions from the determination of EC and β^+ intensities, the energy calibration including the effect of its dependence on γ-ray multiplicity [11,27], and the EC and β^+ detection efficiencies (see Sec. 3.3.4 of Ref. [11]). To our knowledge, this is the first measurement of the Q_{EC} value of ^{97}Ag, which so far has only been estimated from systematic trends to be 7010(400) keV [31]. A comparison with shell-model predictions will be given in Sec. VI A.

V. COMPARISON OF CLUSTER CUBE AND TAS RESULTS

A. γ-intensity distributions

As shown in Fig. 7, the γ-intensity distributions $I_\gamma(E)$ obtained from the Cluster Cube and TAS measurements are in very good agreement. In particular, there is little difference for ^{97}Pd excitation energies below 4 MeV, if the statistical uncertainties are taken into account. As shown in Table II, the difference of the total γ-intensity values determined by the two methods amounts to 8.4(37)% (per β-decay of ^{97}Ag) which, if normalized to the total γ intensities measured by TAS, corresponds to a fraction of only 3.0(15)% of the total β intensity. As far as the average γ multiplicity is concerned, the TAS measurement yields a value of 2.52(5) which is in very good agreement with the value of 2.43(3) obtained from the Cluster Cube data. We note that this difference mainly lies above the ^{97}Pd excitation energy of 4 MeV, where the Cluster Cube measurement has missed a total γ intensity of 8.9(3)% (per β-decay of ^{97}Ag) in comparison to the TAS data.

B. β-intensity distributions

The I_β distribution obtained from deconvoluting the TAS spectra is presented in Fig. 8, together with the Cluster Cube result. Except for some smaller structures, the results from both methods are globally similar, especially for the major peaks including the large resonance between 3 MeV and 4.8 MeV. It is also worth noting that within the uncertainties, we obtained the same I_β value for the $g_{7/2}$ state (686.6 keV) of ^{97}Pd from both measurements. This indicates that the γ-ray transitions feeding this state are evidently so intense that they are quantitatively recorded by the Cluster Cube. However, the Cluster Cube data show a little more β intensity than the TAS data in the region below 4 MeV, while missing some intensity above that energy. As shown in Table II, the two methods yield an I_β difference of 9.0(3)% (per β-decay of ^{97}Ag) above ^{97}Pd excitation energy of 4 MeV. This result can be interpreted as being due to the γ-intensity of 8.9(3)%

TABLE II. Comparison of the results from the Cluster Cube measurement and from the TAS measurement in several regions of ^{97}Pd excitation energies.

^{97}Pd excitation energy (MeV)	γ-intensity [a]		β-intensity [a]		B(GT)	
	Cluster Cube	TAS	Cluster Cube	TAS	Cluster Cube	TAS
0.0–4.0	222.1(34)	220.7(50)	79.1(30)	69.6(30)	0.93(18)	0.88(11)
4.0–5.4	21.2(3)	30.1(30)	20.9(3)	29.1(30)	1.09(22)	1.79(23)
5.4–6.0	0	0.80(15)	0	0.80(15)	0	0.33(9)
0.0–6.0	243.2(34)	251.6(50)	100	99.8	2.02(40)	3.00(40)

[a]Absolute intensity in % per β decay of ^{97}Ag.

(per β-decay of ^{97}Ag) that the Cluster Cube measurement has missed. This deficiency can be related to the sensitivity limit of the detector in general and, in particular, to γ rays emitted from high-lying levels above 4 MeV to states in the range 1.7–3 MeV, as discussed in Sec. V A. The high level density in the relevant range of ^{97}Pd excitation energies and the corresponding fragmentation of the ^{97}Ag β-intensity indeed represent a serious challenge even for such an efficient array as the Cluster Cube.

C. GT-strength distributions

For a pure allowed GT transition, the β strength B(GT) can be calculated according to

$$B(\mathrm{GT}) = \frac{D \cdot I_\beta(E)}{f(Q_{\mathrm{EC}} - E) \cdot T_{1/2} \cdot 100}, \tag{2}$$

where $D = 3860(18)$ s denotes the constant corresponding to the value of the axial vector weak interaction coupling constant g_A for the decay of the free neutron [32,33], I_β the β-intensity value in % per β decay, E the excitation energy of the daughter nucleus, f the phase-space factor, Q_{EC} the total energy released in electron-capture (EC) decay to the ground-state of the daughter nucleus, and $T_{1/2}$ the β-decay half-life.

Using the Q_{EC} value obtained from the TAS data, the half-life of 25.3 s determined previously [21], and the I_β values deduced in this work, we calculated the ^{97}Ag GT strength shown in Fig. 9. The global shapes of the β-strength distributions from Cluster Cube and TAS data are in good agreement, showing a resonance around 4 MeV with a width of approximately 1.8 MeV. If summing the GT strength in the range from 3 MeV to 4.8 MeV which roughly covers the resonance, the difference between the results from the Cluster Cube and TAS data is only about 21%.

As shown in Table II, we obtained a ΣB(GT) value of 2.02(40) (the uncertainty originates mainly from the contribution of the Q_{EC} value) from the Cluster Cube data in comparison to a value of 3.00(40) from the TAS data up to ^{97}Pd excitation energy of 6 MeV. This discrepancy mainly stems from excitation energies above 4 MeV. Above 6 MeV, the TAS has identified some B(GT) strength as can be seen from Fig. 9; however, the related statistical uncertainties are so large that these data are neglected. We conclude that, up to 6 MeV excitation energy of ^{97}Pd, the Cluster Cube data have missed 33(8)% of ΣB(GT) in comparison with the TAS results, which mainly corresponds to the missing β-feeding intensities of 9.0(3)% (per β-decay of ^{97}Ag) for states above a ^{97}Pd excitation energy of 4 MeV. Note that missing even a comparatively small amount of β feeding to high-lying states leads to a large discrepancy of the ΣB(GT) value, due to the strong dependence of the phase-space factor f on the decay energy [see Eq. (2)].

On the one hand, the fact that the ΣB(GT) value observed by the Cluster Cube in this work (2.02) is much larger than that obtained in the previous work (0.44), which was based on standard germanium detectors [21], indeed represents a considerable progress. As shown in Fig. 10, the previous work [21] only reached the tail of the GT resonance. However, the ΣB(GT) value deduced from the Cluster Cube data indicates that even this exceptionally good high-resolution device has not fully met the challenge of investigating such a complex β decay. On the other hand, due to the low energy-resolution, TAS cannot provide the fine-structure of the β intensity in contrast to the Cluster Cube. For example, the

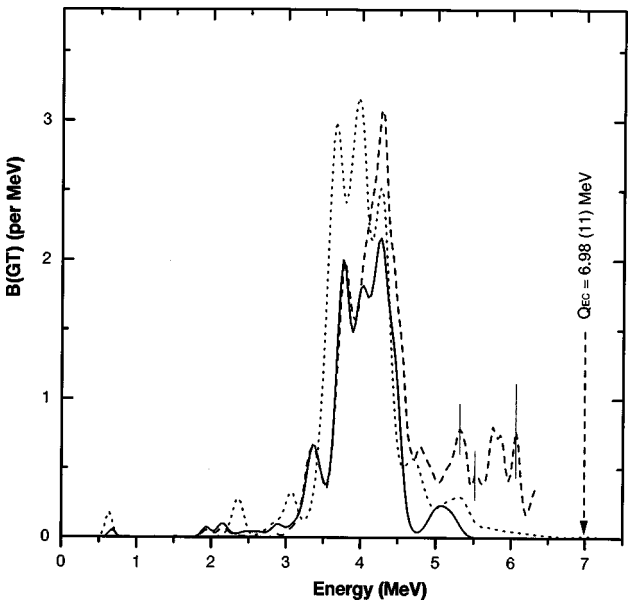

FIG. 9. GT-strength distributions for the decay of ^{97}Ag obtained from the Cluster Cube measurement (solid line), the TAS measurement (dashed line), and the SNB-basis calculation (dotted line). The results from the Cluster Cube measurement and the SNB shell-model calculation were adapted to the TAS resolution by a smoothing procedure. The theoretical GT strength has been reduced by a hindrance factor of 4.3 (see text). The uncertainties shown for the high-energy tail of the TAS data represent the statistical uncertainties. The experimental Q_{EC} value is indicated by an arrow.

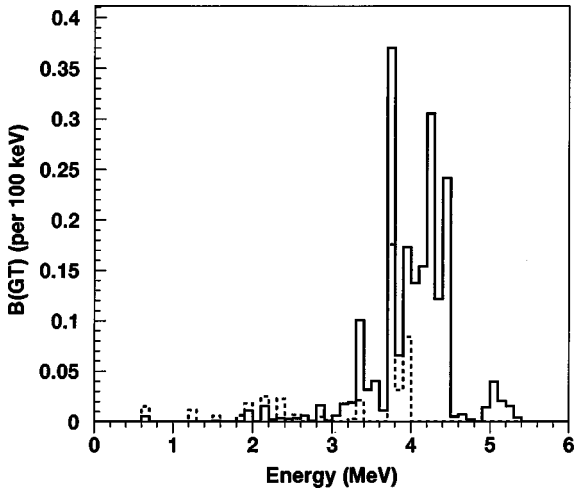

FIG. 10. GT-strength distributions for the decay of ^{97}Ag deduced from the Cluster Cube measurement (solid histogram) and from a previous work [21] (dashed histogram).

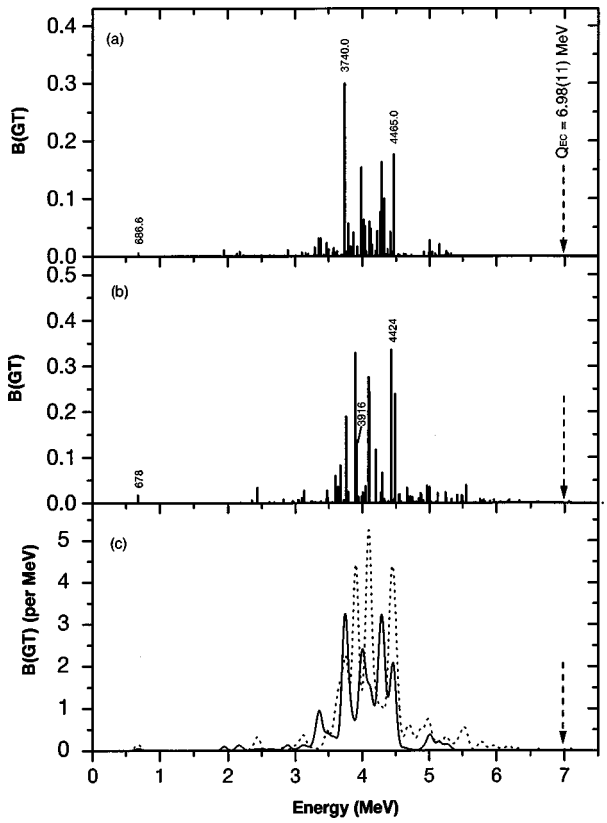

FIG. 11. GT-strength distributions for the decay of ^{97}Ag deduced from the Cluster Cube measurement and the SNC shell-model calculation. The theoretical GT strength has been reduced by a hindrance factor of 4.3 (see text). (a) B(GT) histogram from the Cluster Cube measurement. (b) B(GT) histogram from the SNC calculation. (c) B(GT) distributions from both Cluster Cube measurement (solid line) and SNC calculation (dotted line), smoothed by using a Gaussian function with a FWHM of 100 keV. The energies of some representative levels are given in keV. The experimental Q_{EC} value is indicated by arrows.

TAS data do not resolve the entire peak structure of the GT-strength distribution in the resonance, as shown in Fig. 11. This advantage of the Cluster Cube data will be further discussed in Sec. VI together with a shell-model calculation. Moreover, the deconvolution of the TAS spectra depends strongly on knowing the response function of the TAS for each decay under investigation. To obtain the response function, the decay scheme is desirable, which can only be provided by high-resolution studies. The more complete the obtained decay scheme is, the less assumptions one has to make in unfolding TAS spectra and thus the more reliable are the I_β and the GT-strength distributions determined by means of TAS.

VI. DISCUSSION

A. Gross structure of GT-strength distribution and GT quenching

The theoretical interpretation of the GT strength is based on starting with a closed-shell configuration for ^{100}Sn where the orbitals $0s$, $0p$, $0d1s$, $0f1p$, and $0g_{9/2}$ for both protons and neutrons are filled. The simplest model for the ^{97}Ag ground-state has three proton holes in the $0g_{9/2}$ orbital. Then Eq. (1) with $N_{9/2}=7$ and $N_{7/2}=0$ gives a total GT strength of 12.45.

The shell-model analysis of the strength distribution was performed by using a basis and a Hamiltonian that are denoted by SNB and have been discussed in [13]. The *SNB model space* consists of the $1p_{1/2}$, $0g_{9/2}$, $0g_{7/2}$, $1d_{5/2}$, $1d_{3/2}$, $2s_{1/2}$ and $0h_{11/2}$ orbitals. The *SNB basis* consists of a limited set of configurations within the SNB model space in which the active protons are restricted to the $1p_{1/2}$ and $0g_{9/2}$ orbitals, the $1p_{1/2}$ and $0g_{9/2}$ orbitals for neutrons are always filled and the active neutrons are restricted to the $0g_{7/2}$, $1d_{5/2}$, $1d_{3/2}$, $2s_{1/2}$, and $0h_{11/2}$ orbitals. (The results obtained in the calculations within the SNB basis with the SNB Hamiltonian will be referred to simply as the *SNB* results.) Due to these restrictions, Eq. (1) is still valid, even though the SNB basis goes beyond the extreme single-particle shell model by including proton holes in the $1p_{1/2}$ orbital. The value of $N_{9/2}$ increases from 7 to 7.24 and the total GT strength from Eq. (1) becomes 12.88, i.e., slightly larger than that derived from the simplest model mentioned above. In the following discussion, we consider the SNB value as a reference, which, when compared with the experimental strength of 3.0(4), gives a hindrance factor of 4.3(6).

The GT-strength distribution obtained with the SNB basis and Hamiltonian are compared with experiment in Fig. 9. The position and width are in qualitative agreement with experiment, but quantitatively the position of the peak is a few hundred keV low compared to experiment. The position of the peak is determined by the spacing between the $0g_{9/2}$ proton and $0g_{7/2}$ neutron single-particle energies and by the particle-hole (neutron-proton) interaction strength. For the SNB Hamiltonian the particle-hole interaction was that obtained from a bare G matrix and then reduced by a factor of $N_{pn}=0.7$ in order to improve the Z dependence of the splitting between the $1d_{5/2}$ and $0g_{7/2}$ neutron single-particle energies (as determined by the position of the lowest $5/2^+$ and $7/2^+$ states in the odd-even nuclei with $N=51$). Better agreement with the centroid of the GT-strength distribution can be achieved by increasing the particle-hole normalization to $N_{pn}=0.77$. This 10% increase would give a Z dependence for the $1d_{5/2}$-$0g_{7/2}$ splitting which is still acceptable. The GT-strength distribution obtained with this new interaction, which we will call SNC, is shown in Fig. 12. Since the particle-hole interaction does not change the ^{97}Ag ground state, the total GT strength is the same for SNB and SNC Hamiltonians, the only difference is in the details of the strength distribution. In this section we discuss the total GT strength and in the next section we discuss some of the details of the decay scheme.

The present experiment is sensitive up to a region of excitation energy (6 MeV) which is beyond the peak of the theoretical distribution and which accounts for 98% of the total theoretical strength. It is possible that configuration mixing beyond the SNB basis would result in more GT strength above 6 MeV, but such calculations for this mass region have not yet been carried out. For the $0f1p$ shell it is

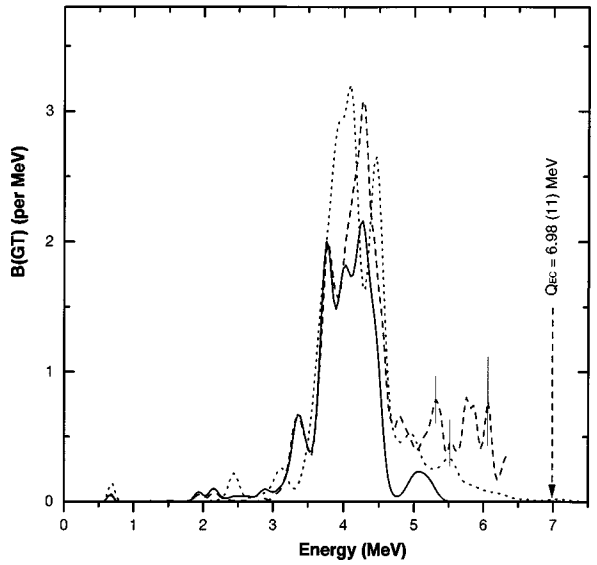

FIG. 12. GT-strength distributions for the decay of ^{97}Ag obtained from the Cluster Cube measurement (solid line), the TAS measurement (dashed line) and the SNC shell-model calculation (dotted line). The results from the Cluster Cube measurement and the SNC calculation were adapted to the TAS resolution by a smoothing procedure. The theoretical GT strength has been reduced by a hindrance factor of 4.3 (see text). The uncertainties shown for the high-energy tail of the TAS data represent the statistical uncertainties. The experimental Q_{EC} value is indicated by an arrow.

possible to compare the results obtained with restricted configuration-mixing (equivalent to the SNB basis) and unrestricted configuration-mixing (Monte Carlo) calculations (equivalent to the the full SNB model space). This comparison suggests that going to the unrestricted configuration mixing does not significantly change the shape of the distribution, but it does *reduce* the total β^+ strength (compare, for example, Figs. 10 and 11 in [34] to Fig. 4 in [35]).

We now turn to a discussion of the total GT strength by using results from core polarization and Monte Carlo calculations for $N=50$ isotones between ^{100}Sn and ^{96}Pd, and by confronting them with the experimental data available for ^{98}Cd, ^{97}Ag, and ^{96}Pd. The GT hindrance factors h deduced from this comparison, which are shown in Table III, are restricted to the GT strength within the respective Q_{EC} value. In the case of ^{97}Ag, we believe that the value of $h=4.3(6)$ is indeed reliable, since most of the GT strength predicted by the SNB calculation lies within the experimentally accessible range of excitation energy, as mentioned above, and since the statistical and systematical uncertainties involved in the TAS measurement have been thoroughly investigated (see Sec. IV C). The situation is different for ^{98}Cd and ^{96}Pd. The measurement of the ^{98}Cd decay [36] is hampered by insufficient experimental sensitivity. The value of $h=3.8(7)$ given in Table III refers to the SNB strength within the sensitivity limit [13]. However, a systematical uncertainty for this procedure has not been included. The problem with the ^{96}Pd decay [37] are partly related to the experimental sensitivity limit again, but also to the small Q_{EC} value of 3450(150) keV. The latter restriction is serious as the SNB calculation predicts a substantial part of the GT strength to populate a ^{96}Rh state at an excitation energy of 2.6 MeV [13]. If one considers the *entire* SNB strength or its fraction up to ^{96}Rh excitation energies of 2.6 or 2.0 MeV, one gets total GT strength of 11.39, 10.56, or 8.95 and h values of 4.9(2), 4.5(2), or 3.9(2), respectively. In a somewhat tentative evaluation of this effect we estimate the h value of ^{96}Pd to be 4.2(5) as indicated in Table III.

The hindrance factor can be broken down into two factors: h_{low}, which involves going from the restricted SNB basis to the unrestricted (full) basis within the SNB model space, and, h_{high}, which comes from higher-order effects beyond the SNB model space. Specifically, h_{low} is defined as the ratio of the total strength obtained in the SNB basis divided by that obtained in the unrestricted SNB model space. h_{high} is the ratio of the total strength obtained in the unrestricted SNB model space divided by that obtained in an exact model which includes all possible baryon and meson configurations (mainly nucleon and Δ particle). For practical reasons, the total strength is defined as that associated with the excitation-energy range expected for the GT final states within the SNB model space. By definition, h_{low} and h_{high} are multiplicative, and the total hindrance factor h is given by $h=h_{low}\cdot h_{high}$.

The effects associated with h_{high} have been studied in lighter nuclei, where it is possible to explicitly include the unrestricted configuration mixing related to h_{low} in the wave functions, and then to compare with experiment to obtain h_{high}. The resulting average value of h_{high} is 1.68 for the sd shell [38] and 1.81 for the fp shell [39]. As h_{high} appears to be approximately independent of state and nucleus, it is thus

TABLE III. GT-hindrance factors for $N=50$ isotones near ^{100}Sn deduced, with reference to the SNB prediction, from experiments and from a theoretical calculation [14,40,15]. The experimental data for ^{96}Pd and ^{98}Cd originate from Ref. [13], whereas those for ^{97}Ag stem from this work. See text for details, in particular concerning the uncertainties of the results for ^{96}Pd and ^{98}Cd.

	Isotope	^{100}Sn	^{99}In	^{98}Cd	^{97}Ag	^{96}Pd
h_{low}	Core-polarization	1.29	1.36	1.59	1.65	2.00
	Monte-Carlo	1.7	(1.8)	2.0	(2.1)	2.5
h	h_{high} × core polarization	2.3	2.4	2.8	2.9	3.5
	h_{high} × Monte Carlo	3.0	(3.1)	3.5	(3.7)	4.4
	Experiment			3.8(7)	4.3(6)	4.2(5)

referred to as a ''global'' hindrance factor. For the discussion below we will take the average $h_{\mathrm{high}}=1.75$.

We will discuss two calculations for h_{low}, the core-polarization calculations of Towner [14] and the Monte Carlo calculations of Koonin *et al.* [15]. Towner calculated the effects due to pairing correlations and core-polarization. The pairing part of Towner's calculation was subsequently found to be too large [40] and will thus not be included [41]. The pairing interaction is included in the SNB and SNC Hamiltonians. Of the three interactions considered in [14], the $\pi+\rho$ interaction of [42] is the most realistic one [41] and will thus be used for the following discussion. We note that Towner used an extreme single-particle shell-model with a pure $g_{9/2}$ proton configuration as a reference. The small difference between this and our SNB reference is neglected. The hindrance factors h_{low} from the core-polarization calculations of Towner are given in Table III. They are not constant but have a Z dependence as well as an odd-even staggering. The smallest hindrance is obtained for ^{100}Sn and becomes larger as one goes away from ^{100}Sn. The effect of the increase away from ^{100}Sn was discussed in [11]. The effect of the odd-even staggering is to make the result for Z_h proton holes in ^{100}Sn similar to that of Z_h+1 proton holes, where Z_h is even. When combined with the global hindrance factor to obtain $h=h_{\mathrm{low}}\cdot h_{\mathrm{high}}$, the results of Towner are about 30% smaller than the experimental results available for ^{98}Cd, ^{97}Ag, and ^{96}Pd, as can be seen from Table III.

The Monte Carlo calculations include correlations which go beyond the core-polarization model. The Monte Carlo hindrance factors also show a Z dependence similar to that of the core-polarization calculations, but were not calculated for the odd-even nuclei. The Monte Carlo results given in brackets in Table III are interpolated assuming the trend as suggested by Towner's core-polarization results. The hindrance factors from the Monte Carlo calculation are larger than the core-polarization results and are in better agreement with the experimental data given in Table III. This comparison suggests that the core-polarization approximation takes into account most but not all of the GT hindrance. However, such comparisons with a consistent set of effective interactions tested against other experimental observables remain to be carried out.

The SNB Hamiltonian gives a Q_{EC} value of 7.024 MeV and a GT β decay half-life of 3.15 s. The SNC Hamiltonian gives 6.937 MeV and 4.64 s, respectively. These Q_{EC} values, as well as those of 6.76 and 7.03 MeV obtained from different shell-model calculations [21,43], are in good agreement with the experimental result of 6.98(11) MeV presented in Sec. IV D. From a comparison of the SNC and experimental half-lives a hindrance factor of 5.6 would be obtained. However, this is weighted strongly by transitions to low-lying states that have small GT strengths but high β intensities. Therefore, the comparison of the total GT strength provides a much better measure of the hindrance.

B. Fine structure of GT resonance

In Fig. 12, the GT-strength distribution from the SNC calculation is compared with the experimental results from the Cluster Cube and TAS measurements. As discussed above, the centroid and width of both experimental results are well reproduced by the SNB calculation. The SNC calculation has a small adjustment in the neutron-proton interaction strength to match the peak position more exactly, but yields the same width as the SNB calculation. There are, however, many details of both SNB and SNC which do not agree with experiment, and here we discuss the comparison for SNC. In terms of the β-decay branching ratios, the most significant one of these is that the SNC calculation predicts too much strength for the decay to the lowest $7/2^+$ state in comparison to the experimental results. The SNC structure of this state is dominated by that of a $0g_{7/2}$ neutron coupled to the ground state of ^{96}Pd. Its B(GT) value is reduced from the single-particle shell-model value 1.78 down to 0.07 due to mixing with the three-quasiparticle configuration and then further down to 0.017 due to the h_{low} and h_{high} correlations. The further mixing needed to bring it down to the experimental value of 0.008 could come from a variety of sources.

The doublet structure around 2 MeV obtained from the experiment does not occur in the calculation which, however, shows a single small B(GT) maximum around 2.5 MeV. The fine structure of the GT resonance in the experimental and theoretical distributions also differs to some extent. In the high-energy tail, we observed about twice as much strength from the TAS data in comparison with the shell-model calculation (from the TAS data we obtained about 24% of the total GT strength above 4.7 MeV).

Due to the poor energy resolution, it is difficult to measure the fine-structure of the GT resonance by using the TAS spectrometer. The Cluster Cube result, however, offers an excellent opportunity for comparing the fine-structure of the GT-strength distribution with the shell-model calculation. In Fig. 11, the B(GT) distributions from the Cluster Cube data and the SNC calculation are shown level by level. The experimental 4465 keV ($9/2^+$) state can be related to the theoretical $9/2^+$ level at 4424 keV. Whereas the experiment gives the most strongly populated level to be at 3740 keV ($11/2^+$), the SNC calculation predicts several levels around 3895 keV, but only the 3916 keV level has a spin of $11/2^+$. It is difficult to find other corresponding levels, which means that, although the shell-model calculation very well reproduces the *global* structure in the GT resonance of ^{97}Ag, the detailed microscopic structure for this decay can not be determined from a comparison between experiment and theory. We regard this partly as being sensitive to more detailed aspects of the interaction as well as being part of a ''statistical'' aspect of the mixing between the final states.

Taking into account the fact that the level energies predicted by the calculation may have uncertainties, we have smoothed the distributions from both SNC calculation and Cluster Cube data by using a Gaussian function with a FWHM of 100 keV, as shown in Fig. 13. The GT strength from the SNC calculation is separated in this figure according to the spin values of $7/2^+$, $9/2^+$, and $11/2^+$, respectively, of the levels populated by allowed GT decay of ^{97}Ag. Among the three components of the resonance predicted by the calculation, that with the highest excitation energy (centroid at 4424 keV) consists almost entirely of $9/2^+$ states. In

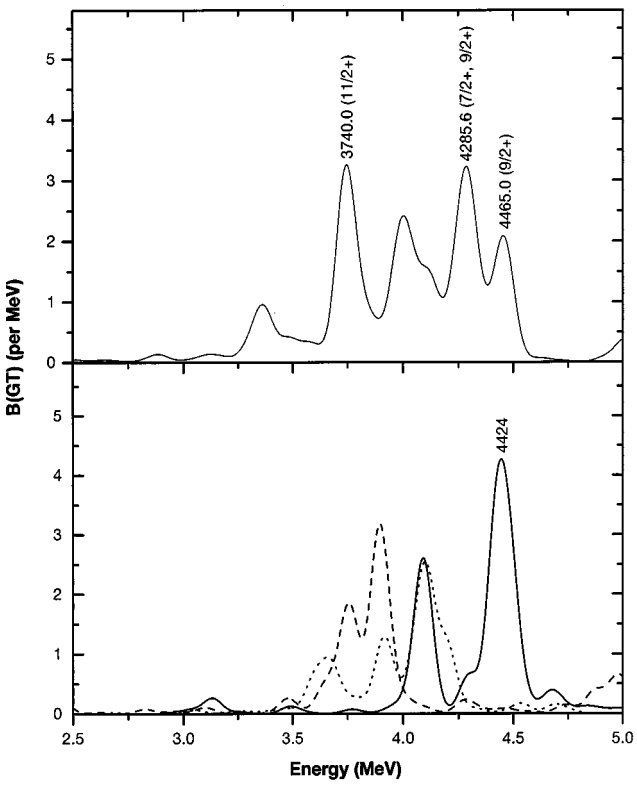

FIG. 13. Part of the GT-strength distributions for the β decay of ^{97}Ag, showing the GT resonance obtained from the Cluster Cube measurement (upper panel) and from the SNC shell-model calculation (lower panel). The theoretical GT strength has been reduced by a hindrance factor of 4.3 (see text). Both distributions are smoothed by using a Gaussian function with a FWHM of 100 keV. The results from the SNC calculation are separated according to the spins of ^{97}Pd states (dashed line for $7/2^+$, solid line for $9/2^+$, and dotted line for $11/2^+$) populated by allowed GT decays of ^{97}Ag. The numbers given on the top of the peaks are the energies in keV of the states populated with the largest GT strength among all states within each peak.

this case, the nucleon-nucleon residual interaction raises mostly the energies of the levels with the intermediate spin resulting from the angular-momentum coupling $(\pi g_{9/2}^{-1}\nu g_{7/2})1^+\otimes\pi g_{9/2}$ following the $\pi g_{9/2}\rightarrow\nu g_{7/2}$ GT transition. Furthermore, the experimental B(GT) distribution contains two high-energy peaks with centroids at 4286 keV and 4465 keV, respectively. The peak centered at 4286 keV mainly consists of three states, whose experimentally deduced spins are $7/2^+$ or $9/2^+$, whereas the peak at 4465 keV is dominated by one $9/2^+$ state. The clear correspondence between the experimental and the theoretical results obtained for the $9/2^+$ states can, however, not be extended to states with other spins. None of the other two peaks of the calculated GT resonance is pure, but contains contributions from states with different spins. Despite the mixture of spins, these two peaks predicted by the shell-model calculation have been confirmed by the experimental measurement, as shown in Fig. 13.

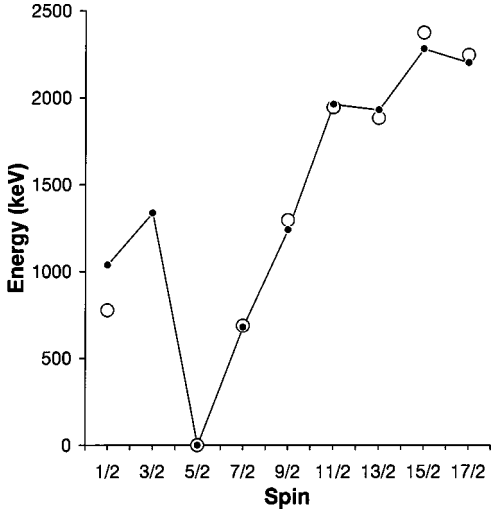

FIG. 14. Energies of the lowest-lying positive-parity states of ^{97}Pd for various spins. Displayed are experimental results (open circles) together with SNC shell-model predictions (full circles). The experimental data are based on the Cluster Cube measurement and previous in-beam works [24,25,23]. The shell-model predictions are connected by straight lines to guide the eye.

C. The first excited $1/2^+$ state of ^{97}Pd

As shown in Fig. 14, the SNC calculation reproduces the energies of the lowest-lying states of ^{97}Pd from $7/2^+$ to $17/2^+$ with an accuracy of better than 100 keV. As the 775 keV level deexcites by a single γ ray to the ground-state $(5/2^+)$, its spin is restricted to values between $1/2^+$ and $9/2^+$. From the point of view of the shell-model calculation, only a $1/2^+$ state at 1036 keV is reasonably close to this state with a difference of 261 keV [predicted states with other spins are at least 464 keV (for $9/2^+$) further away]. Therefore we assume a spin of $1/2^+$ for this state. Checking the neutron $s_{1/2}$ single-particle states in $N=51$ nuclei below ^{97}Pd (no corresponding experimental data are available above ^{97}Pd), we find that the energy of the $1/2^+$ state decreases systematically when adding proton pairs to the $g_{9/2}$ orbital. For ^{91}Zr, the first $1/2^+$ state is situated at 1205 keV [44]. The dominant configuration of this nucleus is characterized by 40 protons filling all orbits below $g_{9/2}$, with that orbit being empty. With two and four protons in the $g_{9/2}$ orbit, ^{93}Mo and ^{95}Ru have their first $1/2^+$ state at 943 and 788 keV, respectively [44]. Therefore, the above-mentioned assignment of $1/2^+$ to the 775 keV state in ^{97}Pd, which has an extra pair of protons in the $g_{9/2}$ orbital in comparison with ^{95}Ru, is in good agreement with this systematic trend, which from shell-model calculations is expected to reverse towards ^{99}Cd and ^{101}Sn [43]. Incidentally, the SNC prediction of the level energy for this ^{97}Pd state agrees with results from another shell-model calculation [43], which predicts also the $1/2^+$ states of $N=51$ nuclei to be 100–200 keV higher than found experimentally.

The SNC calculation predicts the lowest $1/2^+$ level in ^{97}Pd to have about 40% of the $s_{1/2}$ single-particle component. The $s_{1/2}$ single-particle energy assumed for the SNB and SNC Hamiltonians would have to be lowered by about

500 keV in order to bring this level down to 775 keV. Thus, with this first evidence for a $s_{1/2}$ quasiparticle state in $N=51$ isotones beyond the $\pi g_{9/2}$ midshell, the position of the $s_{1/2}$ single-particle state in ^{101}Sn can be estimated to be 1.2–1.6 MeV above the $d_{5/2}$ ground state.

The $1/2^+$ level of ^{97}Pd is populated by γ cascades from higher-lying levels, but may also be fed directly by β decay of ^{97}Ag. These cascades originate from levels with relatively high spins. We have calculated in the SNB model the γ feeding of the $1/2^+$ level from the higher-spin levels populated in the β decay, and find a γ intensity of 0.30 (out of 100 β decays) for the $1/2^+$ to the ground-state transition. The agreement with the experimental value of 0.43(3) is good considering the complexity of the γ-cascades feeding the $1/2^+$ state. It is this complexity which introduces ambiguities in the interpretation of the direct β population of this level: The β intensity of 0.14(3)% per 100 decays [22] was deduced for the $1/2^+$ state from the γ-intensity balance involving exclusively weak transitions, and represents rather an upper limit if unobserved γ feeding is considered. Correspondingly, the $\log ft$ value of 7.70 [22] for the ^{97}Ag β-decay to this $1/2^+$ level represents a lower limit. This result does not allow us to draw a definite conclusion concerning a direct β feeding to this $1/2^+$ state from a so far unobserved $1/2^-$ isomeric state of ^{97}Ag. The unambiguous detection of ^{97m}Ag $(1/2^-)\rightarrow{}^{97}$Pd $(1/2^+)$ β decay, which is of the first forbidden type, would require improved statistics for the determination of the half-life of the 775 keV γ ray, preferably accompanied by a stronger suppression of the ^{97}Pd contamination and the room background. An alternative would be the choice of another reaction mechanism for the production of the $1/2^-$ isomer, in contrast to heavy-ion induced fusion-evaporation which rather selects high-spin states.

VII. SUMMARY

This work describes the first successful attempt to apply two powerful complementary setups, Cluster Cube and TAS, to investigate the β decay of a very neutron-deficient isotope near ^{100}Sn. Good agreement between the results from both measurements has been reached for the whole range of excitation energies in the daughter nucleus.

With the high-resolution spectrometer (Cluster Cube), we observed 603 γ rays (578 new) in the decay of ^{97}Ag, deexciting 151 ^{97}Pd levels (132 new). Using the γ-intensity balances, we obtained the GT-strength distribution, revealing a large resonance around a ^{97}Pd excitation energy of 4 MeV with a width of about 1.8 MeV. Additional detailed information on the β decay of ^{97}Ag has been gained. In particular, we have identified γ-feeding of a high-spin state (2244 keV, $17/2^+$) and a possible low-spin state (775 keV, $1/2^+$), both of which have spins very different from that of the ^{97}Ag ground state.

The result from the high-efficiency device TAS not only confirms the existence of the GT resonance, but also agrees in terms of its global shape. Comparing the results obtained from both techniques, the Cluster Cube measurement failed to observe a total β intensity of 9.0(3)% (per β-decay of ^{97}Ag) above 4 MeV excitation energy of ^{97}Pd, which corresponds to a deficit value of 8.9(3)% (per β-decay of ^{97}Ag) of the β-delayed γ intensity in the same energy region. If normalized to the total γ intensity obtained by TAS, however, only 3.0(15)% of γ intensities remained unobserved in the Cluster Cube measurement for the whole energy region up to 6 MeV, showing the excellent detection sensitivity of the Cluster Cube. However, we are still unable to derive a quantitative experimental sensitivity limit for the β intensity as a function of ^{97}Pd excitation energy, as this depends on the level densities of the excited states and their de-excitation pattern, which are unknown. As far as the summed GT strength is concerned, the Cluster Cube data have missed 33(8)% of the total strength up to 6 MeV which is mainly accounted for by the deficit value of 9.0(3)% (per β-decay of ^{97}Ag) in I_β to the states above 4 MeV.

Shell-model calculations within the restricted SNB basis reproduce the excitation energy and overall shape of the GT-strength distribution despite the discrepancy in $\Sigma B(\mathrm{GT})$. The GT-hindrance factor with respect to the TAS result amounts to 4.3(6), which agrees with the value of 3.7 expected from further configuration mixing within the SNB model space and from the higher-order configuration mixing beyond the SNB model space. This large hindrance factor is a direct indication about the complexity of the actual nuclear wave functions compared to what one expects from the simplest single-particle shell model. By using a combination of high-resolution and low-resolution spectroscopy on nuclei that are close enough to the ^{100}Sn core to apply large scale shell-model calculations, progress has thus been made in understanding the phenomenon of GT quenching.

ACKNOWLEDGMENTS

This work was supported in part by the European Community under Contract No. ERBFMGECT950083, by the Polish Committee of Scientific Research under Grant No. KBN 2 P03B 039 13, by the Russian Fund for Basic Research and the Deutsche Forschungsgemeinschaft under Contract No. 436 RUS113/201/0(R), by the C.I.C.Y.T. (Spain) under Project No. AEN96-1662, and by the U.S. National Science Foundation under Grant No. 9605207. The authors would like to thank the German Euroball Collaboration for making the Euroball Cluster detectors available for this experiment. These detectors were supported by the German BMBF, the KFA Jülich, the GSI Darmstadt, and the MPI-K Heidelberg. B.A.B wishes to thank the Alexander von Humboldt-Foundation for support.

[1] R. Schneider, J. Friese, J. Reinhold, K. Zeitelhack, T. Faesterman, R. Gernhäuser, H. Gilg, F. Heine, J. Homolka, P. Kienle, H. J. Körner, H. Geissel, G. Münzenberg, and K. Sümmerer, Z. Phys. A **348**, 221 (1994).

[2] M. Lewitowicz, R. Anne, G. Auger, D. Bazin, C. Borcea, V. Borrel, J. M. Corre, M. Huyse, Z. Janas, H. Keller, S. Lukyanov, A. C. Mueller, Yu. Penionzhkevich, M. Pfützner, F. Pougheon, K. Rykaczewski, M. G. Saint-Laurent, K. Schmidt, W. D. Schmidt-Ott, O. Sorlin, J. Szerypo, O. Tarasov, J. Wauters, and J. Żylicz, Phys. Lett. B **332**, 20 (1994).

[3] M. Chartier, G. Auger, W. Mittig, A. Lepine-Szily, L. K. Fifield, J. M. Casandjian, M. Chabert, J. Ferme, A. Gillibert, M. Lewitowicz, M. Mac Cormick, M. H. Moscatello, O. H. Odland, N. A. Orr, G. Politi, C. Spitaels, and A. C. C. Villari, Phys. Rev. Lett. **77**, 2400 (1996).

[4] M. Lipoglavšek, J. Cederkäll, M. Palacz, J. Persson, A. Atac, J. Blomqvist, C. Fahlander, H. Grawe, A. Johnson, A. Kerek, W. Klamra, J. Kownacki, A. Likar, L.-O. Norlin, J. Nyberg, R. Schubart, D. Seweryniak, G. de Angelis, P. Bednarczyk, Zs. Dombrádi, D. Foltescu, D. Jerrestam, S. Juutinen, E. Mäkelä, G. Perez, M. de Poli, H. A. Roth, T. Shizuma, Ö. Skeppstedt, G. Sletten, S. Törmänen, and T. Vass, Phys. Rev. Lett. **76**, 888 (1996).

[5] M. Górska, M. Lipoglavšek, H. Grawe, J. Nyberg, A. Atac, A. Axelsson, R. Bark, J. Blomqvist, J. Cederkäll, B. Cederwall, G. de Angelis, C. Fahlander, A. Johnson, S. Leoni, A. Likar, M. Matiuzzi, S. Mitarai, L.-O. Norlin, M. Palacz, J. Persson, H. A. Roth, R. Schubart, D. Seweryniak, T. Shizuma, Ö. Skeppstedt, G. Sletten, W. B. Walters, and M. Weiszflog, Phys. Rev. Lett. **79**, 2415 (1997).

[6] R. J. Tighe, D. M. Moltz, J.C. Batchelder, T. J. Ognibene, M. W. Rowe, and J. Cerny, Phys. Rev. C **49**, R2871 (1994).

[7] R. D. Page, P. J. Woods, R. A. Cunningham, T. Davinson, N. J. Davis, A. N. James, K. Livingston, P. J. Sellin, and A. C. Shotter, Phys. Rev. Lett. **72**, 1798 (1994).

[8] K. Schmidt, Th. W. Elze, R. Grzywacz, Z. Janas, R. Kirchner, O. Klepper, A. Płochocki, E. Roeckl, K. Rykaczewski, L. D. Skouras, and J. Szerypo, Z. Phys. A **350**, 99 (1994).

[9] J. Szerypo, M. Huyse, G. Reusen, P. Van Duppen, Z. Janas, H. Keller, R. Kirchner, O. Klepper, A. Piechaczek, E. Roeckl, D. Schardt, K. Schmidt, R. Grzywacz, M. Pfützner, A. Płochocki, K. Rykaczewski, J. Żylicz, G. Alkhazov, L. Batist, A. Bykov, V. Wittmann, and B. A. Brown, Nucl. Phys. **A584**, 221 (1995).

[10] J. Szerypo, R. Grzywacz, Z. Janas, M. Karny, M. Pfützner, A. Płochocki, K. Rykaczewski, J. Żylicz, M. Huyse, G. Reusen, J. Schwarzenberg, P. Van Duppen, A. Wöhr, H. Keller, R. Kirchner, O. Klepper, A. Piechaczek, E. Roeckl, K. Schmidt, L. Batist, A. Bykov, V. Wittmann, and B. A. Brown, Z. Phys. A **359**, 117 (1997).

[11] M. Karny, L. Batist, B. A. Brown, D. Cano-Ott, R. Collatz, A. Gadea, R. Grzywacz, A. Guglielmetti, M. Hellström, Z. Hu, Z. Janas, R. Kirchner, F. Moroz, A. Piechaczek, A. Płochocki, E. Roeckl, B. Rubio, K. Rykaczewski, M. Shibata, J. Szerypo, J. L. Tain, V. Wittmann, and A. Wöhr, Nucl. Phys. **A640**, 3 (1998).

[12] Z. Janas, H. Keller, R. Kirchner, O. Klepper, A. Piechaczek, E. Roeckl, K. Schmidt, M. Huyse, J. von Schwarzenberg, J. Szerypo, P. Van Duppen, L. Vermeeren, F. Albus, H.-J. Kluge, G. Passler, F. P. Scheerer, N. Trautmann, V. N. Fedoseyev, V. I. Mishin, R. Grzywacz, A. Płochocki, K. Rykaczewski, and J. Zylicz, Phys. Scr. **T56**, 262 (1995).

[13] B.A. Brown and K. Rykaczewski, Phys. Rev. C **50**, 2270 (1994).

[14] I. S. Towner, Nucl. Phys. **A444**, 402 (1985).

[15] S. E. Koonin, D.J. Dean, and K. Langanke, Phys. Rep. **278**, 1 (1997); D. J. Dean, S. E. Koonin, T. T. S. Kuo, K. Langanke, and P. D. Radha, Phys. Lett. B **367**, 17 (1996).

[16] M. Karny, J. M. Nitschke, L. F. Archambault, K. Burkard, D. Cano-Ott, M. Hellström, W. Hüller, R. Kirchner, S. Lewandowski, E. Roeckl, and A. Sulik, Nucl. Instrum. Methods Phys. Res. B **126**, 411 (1997).

[17] J. Agramunt, A. Algora, D. Cano-Ott, A. Gadea, B. Rubio, J.L. Tain, M. Gierlik, M. Karny, Z. Janas, A. Płochocki, K. Rykaczewski, J. Szerypo, R. Collatz, J. Gerl, M. Górska, H. Grawe, M. Hellström, Z. Hu, R. Kirchner, M. Rejmund, E. Roeckl, M. Shibata, L. Batist, F. Moroz, V. Wittmann, and P. Kleinheinz, in *Proceedings of the International Symposium on New Facet of Spin Giant Resonance in Nuclei*, Tokyo, 1997, edited by H. Sakai, H. Okamura, and T. Wakasa (World Scientific, Singapore), p. 150.

[18] Z. Hu, R. Collatz, H. Grawe, and E. Roeckl, Nucl. Instrum. Methods Phys. Res. A **419**, 121 (1998).

[19] R. Kirchner, D. Marx, O. Klepper, V.T. Koslowsky, T. Kühl, P. O. Larsson, E. Roeckl, K. Rykaczewski, and D. Schardt, Nucl. Instrum. Methods Phys. Res. A **234**, 224 (1985).

[20] R. Kirchner, Nucl. Instrum. Methods Phys. Res. B **26**, 204 (1987).

[21] K. Schmidt, P. C. Divari, Th. W. Elze, R. Grzywacz, Z. Janas, I. P. Johnstone, M. Karny, H. Keller, R. Kirchner, O. Klepper, A. Płochocki, E. Roeckl, K. Rykaczewski, L. D. Skrouras, J. Szerypo, and J. Żylicz, Nucl. Phys. **A624**, 185 (1997).

[22] Z. Hu, Ph.D. thesis, GSI Report 99-03 (1999); submitted to Nucl. Data Sheets.

[23] P. Fettweis, P. del Marmol, M. Degreef, P. Duhamel, and J. Vanhorenbeeck, Z. Phys. A **305**, 57 (1982).

[24] W. F. Piel, Jr., D. B. Fossan, R. Ma, E. S. Paul, N. Xu, and J. B. Mcgrory, Phys. Rev. C **41**, 1223 (1990).

[25] D. Alber, H. H. Bertschat, H. Grawe, H. Haas, B. Spellmeyer, and X. Sun, Z. Phys. A **335**, 265 (1990).

[26] D. Cano-Ott, J. L. Tain, A. Gadea, B. Rubio, L. Batist, M. Karny, and E. Roeckl, Nucl. Instrum. Methods Phys. Res. A **430**, 488 (1999).

[27] D. Cano-Ott, J. L. Tain, A. Gadea, B. Rubio, L. Batist, M. Karny, and E. Roeckl, Nucl. Instrum. Methods Phys. Res. A **430**, 333 (1999).

[28] L. Batist, A. Bykov, V. Janovsky, and V. Wittmann, Report No. LNPI No. 1547, Gatchina (1989).

[29] GEANT: Detector description and simulation tool, CERN Program Library W5013, Geneve, 1994.

[30] N. B. Gove and M. J. Martin, Nucl. Data Tables **10**, 206 (1971).

[31] G. Audi and A. H. Wapstra, Nucl. Phys. **A595**, 409 (1995).

[32] E. Klempt, P. Bob, L. Hornig, J. Last, S. J. Freedman, D. Dubbers, and O. Schärpf, Z. Phys. C **37**, 179 (1988).

[33] S. J. Freedman, Comments Nucl. Part. Phys. **19**, 209 (1990).

[34] W. P. Alford, B. A. Brown, S. Burzynski, A. Celler, D. Frekers, R. Helmer, R. Henderson, K.P. Jackson, K. Lee, A. Rra-

hav, A. Trudel, and M. C Vetterli, Phys. Rev. C **48**, 2818 (1993).
[35] P.B. Radha, D.J. Dean, S.E. Koonin, K. Langanke, and P. Vogel, Phys. Rev. C **56**, 3079 (1997).
[36] A. Płochocki, K. Rykaczewski, T. Batsch, J. Szerypo, J. Żylicz, R. Barden, O. Klepper, E. Roeckl, D. Schardt, H. Gabelmann, P. Hill, H. Ravn, T. Thorsteinsen, I. S. Grant, H. Grawe, P. Manakos, L. D. Skouras, and the ISOLDE Collaboration, Z. Phys. A **342**, 43 (1992).
[37] K. Rykaczewski, I. S. Grant, R. Kirchner, O. Klepper, V. T. Koslowsky, P. O. Larsson, E. Nolte, G. Nyman, E. Roeckl, D. Schardt, L. Spanier, P. Tidemand-Petersson, E. F. Zganjar, and J. Żylicz, Z. Phys. A **322**, 263 (1985).
[38] B. A. Brown and B. H. Wildenthal, Annu. Rev. Nucl. Part. Sci. **38**, 29 (1988).
[39] G. Martinez-Pinedo, A. Poves, E. Caurier, and A. P. Zuker, Phys. Rev. C **53**, R2602 (1996).
[40] I.S. Towner, in *Proceedings of the 5th International Conference on Nuclei far from Stability*, Ontario, 1987, edited by I.S. Towner, AIP Conf. Proc. No. 164 (AIP, New York, 1987), p. 593.
[41] I.S. Towner (private communication).
[42] I.S. Towner and F. C. Khanna, Nucl. Phys. **A399**, 334 (1983).
[43] H. Grawe, R. Schubart, D. Alber, R. Alfier, D.B. Fossan, J. Heese, H. Kluge, K.H. Maier, and M. Schramm, Prog. Part. Nucl. Phys. **28**, 281 (1992).
[44] *Table of Isotopes*, 8th ed., edited by R.B. Firestone and V.S. Shirley (Lawrence Berkeley National Laboratory, University of California, 1996).